Electrical sensing of the dynamical structure of the planetary boundary layer

Article

Published Version

It is advisable to refer to the publisher's version if you intend to cite from the work. See Guidance on citing.

CentAUR

Central Archive at the University of Reading

Reading's research outputs online

Electrical sensing of the dynamical structure of the planetary boundary layer

K.A. Nicoll[a,b,*], R.G. Harrison[a], H.G. Silva[c], R. Salgado[d], M. Melgâo[d], D. Bortoli[d]

[a] Department of Meteorology, University of Reading, Earley Gate, Reading, Berkshire RG6 6BB, UK
[b] Department of Electronic and Electrical Engineering, University of Bath, Claverton Down, Bath BA2 7AY, UK
[c] Renewable Energies Chair, University of Évora, Palácio do Vimioso, Largo Marquês de Marialva, 7002-554 Évora, Portugal
[d] Departamento de Física, ICT, Instituto de Ciências da Terra, Universidade de Évora, Rua Romão Ramalho 59, 7002-554 Évora, Portugal

ABSTRACT

Turbulent and convective processes within the planetary boundary layer are responsible for the transport of moisture, momentum and particulate matter, but are also important in determining the electrical charge transport of the lower atmosphere. This paper presents the first high resolution vertical charge profiles during fair weather conditions, obtained with instrumented radiosonde balloons over Alqueva, Portugal during the summer of 2014. The short intervals (4 h) between balloon flights enabled the diurnal variation in the vertical profile of charge within the boundary layer to be examined in detail, with much smaller charges (up to 20 pC m^{-3}) observed during stable night time periods than during the day. Following sunrise, the evolution of the charge profile was complex, demonstrating charged ultrafine aerosol, lofted upwards by daytime convection. This produced charge up to 92 pC m^{-3} up to 500 m above the surface. The diurnal variation in the integrated column of charge above the site tracked closely with the diurnal variation in near surface charge as derived from a nearby electric field sensor, confirming the importance of the link between surface charge generation processes and aloft. The local aerosol vertical profiles were estimated using backscatter measurements from a collocated ceilometer. These were utilised in a simple model to calculate the charge expected due to vertical conduction current flow in the global electric circuit through aerosol layers. The analysis presented here demonstrates that charge can provide detailed information about boundary layer transport, particularly in regard to the ultrafine aerosol structure, that conventional thermodynamic and ceilometer measurements do not.

1. Introduction

The effect of meteorological processes on the electrical state of the atmosphere has been known about for almost 250 years, even leading Lord Kelvin to suggest that weather forecasting would one day be achieved with an electrometer (e.g. Aplin and Harrison, 2013). The complexity, however, of relationships between atmospheric electrical variables and meteorological processes makes this difficult. What has become evident is that the same meteorological processes that act to transport heat, momentum, moisture and pollutants within the lower atmosphere also transport charge (see review by Hoppel et al., 1986). This has led to suggestions that so-called atmospheric electrical "convection currents" can be used as a method for determining turbulent transport processes in the lower atmosphere, e.g. Markson et al. (1981). The similarity between the convective flux of charge and turbulent transport processes is particularly strong near the surface, i.e. within the planetary boundary layer (PBL). The PBL is the lowest portion of the atmosphere which is directly influenced by the presence of the surface (often referred to historically in atmospheric electricity as the Exchange

or Austausch layer), with a depth ranging from a few hundred meters to several km, varying with latitude and time of day (e.g. Stull, 2012). In the PBL, air-surface interactions take place in the form of mechanical and thermal forces, which drive turbulence and convection respectively. The PBL structure evolves considerably throughout the day (see e.g. Garratt, 1994 for example vertical profiles), and also varies between land and ocean surfaces (e.g. Kaimal and Finnigan, 1994). Processes within the PBL control transport of aerosol particles, moisture and momentum and the PBL top is typically characterised by a temperature inversion (known as a "capping inversion"), which traps these quantities beneath it. The height of the PBL is often used to characterise the vertical extent of mixing within the boundary layer and the level at which exchange with the free troposphere occurs.

Free charge is ubiquitous in the atmosphere and is released by ionisation from Galactic Cosmic Rays (GCRs) and radioactivity near the earth's surface (i.e. gamma and beta radiating directly from the surface, as well as radiation from radioactive gases). This ionisation gives rise to the electrical conductivity of air, σ, which is primarily due to the presence of small cluster ions (nm diameter) (e.g. Tammet, 1995).

Maintenance of charge within the atmosphere is a continual balance between ion generation and loss processes (Hoppel and Frick, 1986). As well as generation of ions by GCRs and radioactivity, ions are destroyed by ion-ion recombination (i.e. self-neutralisation), and lost by attachment to larger particles such as aerosol and cloud droplets. Ions are subject to the same turbulent eddies that transport momentum, moisture and pollutants throughout the PBL. Thus atmospheric electrical variables within the PBL depend on the local ionisation profile, aerosol size and number distribution as well as turbulent mixing of both ions and radioactive gases. Therefore they are heavily dependent on the combined influences of surface drag, heating, and evaporation from the underlying Earth's surface.

As well as being influenced by local meteorological variations, atmospheric electrical variables are also governed by global scale current flow in the global electric circuit, GEC, (e.g. Williams, 2009; Rycroft et al., 2008). This is most evident when studying the diurnal variation in atmospheric electric field, which is usually measured as the Potential Gradient, PG.[1] In clean air PG exhibits a minimum at ~0400 UT and a maximum at ~1900 UT, in accordance with the diurnal variation in global thunderstorm activity (Wilson, 1921; Whipple, 1929; Mach et al., 2011). The globally-invariant nature of this variation, at least on average, was first observed on the ocean cruises organised by the Carnegie Institution (Harrison, 2013), and hence is often referred to as the *Carnegie curve*. GEC effects on surface measurements of PG made within the PBL are often masked by dominant local meteorological effects such as convection or turbulent mixing, which can manifest themselves as additional fluctuations superimposed on the fair weather Carnegie curve (e.g. Israel, 1955). This is of particular importance during summer sunrise when convection causes mixing of the layer of positive charge which can form close to the nocturnal surface (known as the electrode layer[2]), thereby transiently disturbing the established local PG. Electrode layers only occur within a few meters of the surface most commonly over the calm ocean surface where there is no source of radioactive ionisation, but also over land during stable, low wind conditions (Crozier, 1963).

Although positive and negative ions are initially created in equal numbers, natural processes act to separate the different charge polarities, including the transfer of charge to aerosol and cloud droplets. This gives rise to the space charge density, ρ, which refers to the net difference between positive and negative charge per unit volume. ρ is not concerned with the nature of individual charge carriers, but only the total charge retained by all charge carriers. ρ is defined as

$$\rho = e \left[(n_+ - n_-) + \sum_{i=1}^{i=k} \sum_{j=-\infty}^{\infty} jN_{i,j} \right],$$

(1)

where the first term is the ionic space charge contribution and the second term is that due to particulate aerosol. e is the magnitude of the electronic charge, n_+ and n_- are the small ion number concentrations, and the aerosol size distribution is represented by k size categories, each of which spans j elementary charges. Charge separation can arise from flow of the air-Earth conduction current, J_c, which flows vertically between the ionosphere to Earth's surface through aerosol and cloud layers. The theory behind such phenomenon is described in detail in Zhou and Tinsley (2007), Harrison et al. (2015), and Nicoll and Harrison (2016).

Analytical studies of the influence of meteorological processes on atmospheric electric variables date back before the 1800s (e.g. Cavello, 1777), but since most measurements were performed near the surface,

at low altitudes, these sites were almost always within the PBL. To study the effect of the PBL on atmospheric electricity, one must get above the inversion layer, thereby such as through mountaintop observatories, airborne measurements, or very tall towers (such as the Eiffel tower (e.g. Harrison and Aplin, 2003)). The pioneering aircraft measurements of Sagalyn and Faucher (1954, 1956) were amongst the first to demonstrate quantitatively that the electrical conductivity of air aloft was substantially reduced by the presence of aerosol particles trapped within the PBL, with a distinct change in behaviour in the free troposphere above. This was also found through mountaintop observations at the Zugspitze using an instrumented cable car (Reiter and Sládkovič, 1970). Moore et al. (1962) analysed hourly aircraft profiles of space charge (i.e. the net difference between positive and negative charge) throughout the day, demonstrating the similarity between this and the evolution of the PBL temperature profile, as well as the relation to fog and haze layers. More recently, Marshall et al. (1999) have studied the evolution of the electric field profile up to several hundred metres, demonstrating the existence of elevated layers of space charge close to the ground in the build up to sunrise.

In terms of quantifying the relationships between atmospheric electrical variables and turbulent diagnostic parameters, Markson et al. (1981), demonstrated good correlation between aircraft observations of the electrical eddy flux of space charge (found from PG measurements) and surface moisture flux over the ocean surface. In addition, several attempts at characterising the eddy diffusion coefficient (which represents the ability of turbulent eddies to transport atmospheric variables from a region of excess to a region of deficit) have been made both over land (e.g. Kawano, 1957; Kulkarni, 2010) and over the ocean (Hoppel and Gathman, 1971). The ocean situation is more straightforward to analyse due to the absence of radioactivity and low aerosol content, as well as reduced surface roughness.

Much of the modelling work studying atmospheric electricity in the PBL has focused on the electrode layer (Hoppel and Gathman, 1971; Willett, 1979; Willett, 1981; Kulkarni, 2010) as this is one of the main sources of local space charge in the atmosphere. Turbulent scenarios involving the electrode layer are complex, however, Hoppel and Gathman (1972) demonstrated reasonable agreement between a model of the turbulent electrode layer and observations over an ocean surface. More recent work over continental surfaces has demonstrated the existence of sub-mesoscale electrical structures superimposed on the mean wind flow in the PBL, which have been termed "Aero Electric Structures (AES)" (Anisimov et al., 1994) and are directly related to transport of turbulent eddies. These have typical dimensions of 500 to 1000 m and lifetimes of tens of minutes, detected experimentally from high frequency analysis of PG data. Anisimov et al. (1999, 2013) discuss the development of a detailed numerical model for AES formation which takes into account turbulent transport of space charge by convection and demonstrates that the dynamic and stability conditions of the PBL are key to controlling the evolution of the space charge profile.

This work presents new high resolution vertical profiles of space charge through and above the PBL in fair weather conditions. Measurements were made during the ALEX2014 field campaign in Portugal, during the summer of 2014, and consisted of surface measurement of Potential Gradient (PG), as well as a number of specially instrumented radiosonde balloon flights, carrying space charge sensors. Detailed analysis of the diurnal variation in the vertical profile of space charge is undertaken, as well as its relation to the surface PG and ceilometer measurements of aerosol backscatter. This is the first time that inexpensive, disposable electrical sensors have been demonstrated to provide indirect information about turbulent mixing processes in the lower atmosphere.

2. Methodology and instrumentation

The observations described here took place as part of the ALEX2014 field campaign (alex2014.cge.uevora.pt.) at the Alqueva reservoir,

---

[1] The Potential Gradient F is related to the vertical component of the electric field E_z by $F = -E_z$.

[2] The electrode layer results from the flow of ions under the atmospheric electric field (positive ions are driven downward, and negative ones upward) and the presence of the boundary of the surface. At this boundary positive ions flowing downward are forced to stop leading to a net accumulation of positive charge.

Portugal (38.27°N, 7.53°W) during July 2014. The main aim of the campaign was to study the impact of the reservoir on the local environment. Alqueva experiences a typical Mediterranean climate, with warm, dry summer periods, and sparse vegetation. The location of Alqueva is rural, with little anthropogenic pollution. The Alqueva reservoir is the largest inland lake in Portugal, of area 250 km² and 80 km from end to end. The size of the reservoir means that it is common for a lake breeze effect to develop during calm conditions when the lake/land temperature contrast is strong (e.g. see Potes et al., 2017). As this has been shown to affect local meteorological and electrical conditions close to the lake shore (Lopes et al., 2016), we also consider potential lake breeze effects here.

Surface PG measurements were made continuously throughout the campaign (see Lopes et al., 2016) using a JCI 131F electrostatic field mill at 2 m above the ground. The measurement site was located ~100 m from the shoreline at the southern end of the lake, on a small hill ~50 m above the water surface (Parque Solar). A map of the Alqueva reservoir and the location of the measurement at Parque Solar are provided in Appendix A. The field mill was set to a 0–2 kVm^{-1} range, with data sampled at 1 s and logged at 1 minute averages. Nearby meteorological measurements of temperature, relative humidity (RH), wind speed, wind direction and solar radiation were also made. Further instrumentation was used to provide information about the aerosol content at Alqueva in the form of a CL31 Ceilometer manufactured by Vaisala and a TSI Optical Particle Sizer (model OPS3330). The main features of these systems and the data processing and retrieval techniques are described in Appendices C and D.

Balloon-carried instruments were launched from a location ~100 m from the PG measurement site. Vaisala RS92 radiosondes were instrumented with the PANDORA system (Programmable ANalogue and Digital Radiosonde Accessory) developed by the University of Reading (Harrison et al., 2012), which provides a data acquisition system with which to interface additional science sensors to the standard meteorological radiosonde. Each sensor package carried a space charge sensor based on the design described in Nicoll (2013) (simplified to omit the self-calibrating mode). This charge sensor uses a spherical electrode connected to a sensitive electrometer circuit to measure the displacement current generated from a changing electric field, dominated by vertical electric field variations as the sonde ascends. The space charge is derived from the electrometer current and the ascent rate. Calibration details are given in Nicoll and Harrison, 2016. The typical 5 ms^{-1} ascent rate of the sonde, and 1 Hz sampling rate of the PANDORA system provides a measurement approximately every 5 m in altitude. An Intense Observation Period (IOP) during the ALEX2014 campaign took place on 22nd to 24th July 2014 when a total of 8 specially instrumented radiosonde packages were launched during the two days. Balloon flight details during the IOP are given in Table 1.

Sensor packages were flown beneath 600 g balloons, reaching, on average, altitudes of 31 km at burst. An example of a full height vertical profile from one of the specially instrumented radiosondes is shown in Fig. 1 which displays (a) temperature and RH data and (b) space charge

density measured by the charge sensor. Considering the space charge profile, Fig. 1(b) clearly shows that the magnitude of the charge is large within the boundary layer but decreases markedly with altitude above this. The remainder of this paper is concerned with the vertical variation of space charge within the PBL.

3. Results

3.1. Diurnal variation of space charge with height in the PBL

During the most intensive period of the campaign, the specially instrumented radiosondes were launched approximately every 4 h which provides an opportunity to study the time evolution of the vertical profile in space charge as the PBL evolves throughout the day. The period of interest examined further is from 0200 UT 23rd July to 0200 UT 24th July (flights 3 to 8 in Table 1), with individual plots from each flight shown in Fig. 2. The weather during this period was characterised by anticyclonic conditions (surface pressure > 990 hPa for the entire IOP), with clear skies during the day and maximum air temperatures up to 38 °C. Overnight, the clear skies led to rapid cooling (minimum night time temperatures ~16 °C) and the formation of short lived cloud layers lasting only a few hours, which dissipated by 0700 UT most mornings. The 23rd July was dominated by a weak north westerly flow, which was sufficient enough to prevent any lake breeze effect from developing. This is in contrast to the previous day (22nd July), when the strongest lake breeze effect of the entire ALEX campaign was observed (see Potes et al., 2017 for more detail). The effect of the lake breeze on the meteorological conditions on 22nd is discussed in Section 3.2.

Fig. 2 shows thermodynamic quantities of temperature, potential temperature, relative humidity, (RH), horizontal wind speed and direction, as well as magnitude of space charge profiles for six ascents within a 24 hour period on 23rd July. The modulus of the space charge is used here due to the high degree of variability in the space charge measurement which makes the polarity difficult to interpret, which is partly a consequence of measuring at such high resolution. To make the space charge determination as robust as possible, we therefore use the absolute value of space charge. This is an alternative to providing an average profile which would remove the detailed vertical structure in the space charge, which is the main focus here.

Starting with the first ascent at 0208 UT on 23rd July (Fig. 2(a)), the temperature profile in the lower levels is characteristically stable, with a substantial inversion at ~300 m (associated with the formation of the nocturnal boundary layer), with a subsequent smaller near neutral residual layer up to ~2.5 km. The inversions at 2.5 and 3 km are likely to be associated with the remainder of the PBL top from the previous afternoon. The wind profile from the radiosonde demonstrates the presence of two jets between ~0.3–0.7 km and 2–3 km, with a maximum wind speed at 2.3 km. Substantial wind shear (confirmed by the vertical change in wind direction) is also evident at the top of the lower level jet at ~1 km. The space charge profile shows at least 3 distinct

Table 1
Summary of details of specially instrumented balloons launched during the IOP between 22nd and 24th July. Balloon launch times are given in UT which is 1 h behind local time. PBL height is derived according to the most significant inversion in the potential temperature profile. Max space charge is the maximum magnitude of space charge in the layer from the surface up to 3.5 km.

Flight number	Date	Launch time (UT)	PBL height (m)	Max space charge (pC m^{-3})
1	22/07/14	1134	1928	46.5
2	22/07/14	2030	2210	27.3
3	23/07/14	0208	317	23.2
4	23/07/14	0830	704	41.9
5	23/07/14	1130	811	44.5
6	23/07/14	1420	1733	91.7
7	23/07/14	1725	1774	73.6
8	24/07/14	0215	604	79.2
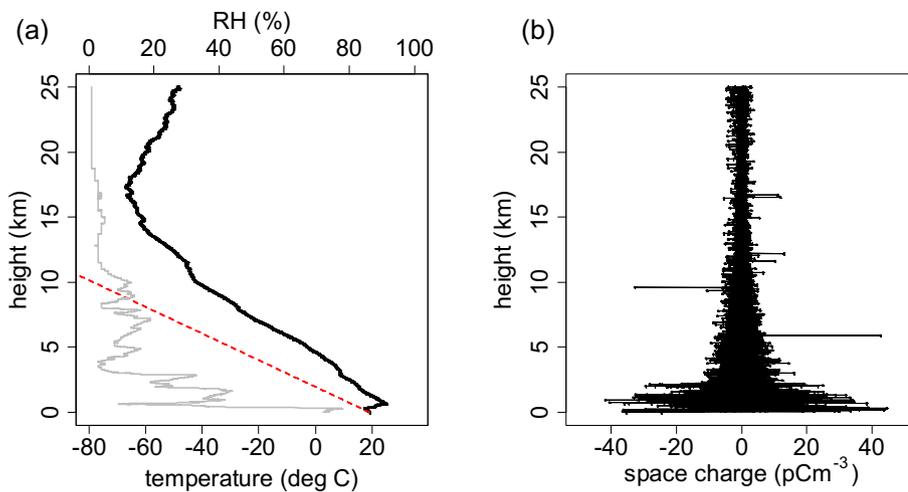
thin layers of charge from the surface up to the inversion at 2.5 km, with a maximum value of ~ 23 pC m^{-3}. The charge layer at 2 km is suggested to result from trapping of charge underneath the main inversion of the residual layer, transported upwards from the surface from the earlier daytime convection. The layer at 1 km is not associated with a temperature inversion, but is coincident with a region of increased RH and wind shear.

Fig. 2(b) shows an ascent profile 6 h later at 0830 UT, by which time the surface layer has become convective; at 300 m the temperature inversion has strengthened, and the charge profile has become much more complex. During the 6 hour period between ascents a number of notable meteorological and solar changes occurred. Fig. 3 shows a time series of ceilometer backscatter during the IOP on 23rd and 24th July 2014. Deep blue areas indicate small backscatter signals demonstrating the absence of clouds, whereas colours from light blue through to red illustrate increasing backscatter values which represent an increase in the atmospheric optical depth. It is clear from the red backscatter between 0530 UT and 0800 UT on 23rd July that a shallow layer of cloud formed at ~ 600 m altitude during the early morning hours, between the balloon ascents. The remnants of this are also apparent from the RH data in Fig. 2(a) and (b) in which the maximum value of RH in the near surface layer increased from 60 to 76% between the 0200 UT and 0830 UT ascents. This occurred due to substantial cooling near the surface under clear skies. The lifetime of the cloud layer was very short, with dissipation by 0800 UT, due to the increase in surface heating (as well as warming from above the cloud) due to the sunrise at 0627 UT.

The space charge profile measured at 0830 UT is clearly very different from the night time profile at 0200 UT. The magnitude of the charge up to 2 km is $\sim$ twice as large as during the earlier ascent, with much deeper individual charge layers, extending from the surface up to 2 km. The most straightforward explanation is that the extra charge originated from horizontal advection, in the large scale synoptic flow. Fig. 4(a) and (b) shows modelled wind speed and direction plots for 1300 UT on 22nd and 23rd July at the surface over Alqueva dam using the non-hydrostatic Meso-NH (Lafore et al., 1998) atmospheric model at 1 km horizontal resolution. (The model and the setup of the simulation are described further in Appendix A.) Considerable differences in the wind conditions exist between the two days in that July 22nd is dominated by a local lake breeze (characterised by wind directions flowing from the centre of the lake to the shore), whilst July 23rd is dominated by a moderate north westerly flow. The increased space charge at 0830 UT on 23rd July is therefore likely to be linked to the advection of air which would have passed over more populated areas such as Lisbon and therefore contained a higher concentration of pollutants than would be present at Alqueva.

An additional contribution to the vertical charge profile at 0830 UT

could arise from the earlier cloud layer at ~ 600 m, which would cause charge to accumulate on the horizontal cloud edges as a result of vertical conduction current flow in the GEC (see Section 3.3 for further discussion). Such charging has been observed to occur frequently due to the conductivity gradients present around stratiform cloud layers (e.g. Nicoll and Harrison, 2010, 2016) as well as aerosol layers (e.g. Moore et al., 1962), and leads to a net charging of droplets/particles in these areas. Although the droplets would evaporate as the cloud dissipates, the charge would be retained either in the form of small ions or on Cloud Condensation Nuclei (CCN) following ion-particle attachment; CCN typically have lifetimes of tens of minutes to hours.

Following the 0830 UT flight, Fig. 2(c) shows the subsequent measurements made at 1130 UT. The nocturnal inversion layer has almost been completely eroded by surface heating, being replaced by a convective boundary layer with a depth of ~ 900 m and the near surface RH reduced to below 50%. The elevated layers of charge observed in the previous flight are still observed, although the uppermost charge layer at 2 km contains a reduced charge density. There is also an enhancement of the charge at ~ 500 m, which is coincident with a substantial vertical change in wind direction, and therefore wind shear.

By 1420 UT (Fig. 2(d)) a substantial charge layer has formed from 100 m to 600 m and strengthened in magnitude to 100 pC m^{-3}. The fact that the temperature profile in the lowest 1.5 km follows the Dry Adiabatic Lapse Rate (DALR, or Γ_d, as shown by the red dashed line) almost exactly, suggests that by this time of day the boundary layer is effectively well mixed, however, this is certainly not the case for the charge profile. An explanation for the increased magnitude of charge in the lowest several hundred meters may be seen in Fig. 5(a), which shows the time series of aerosol concentration and Potential Gradient (PG) measured at Alqueva 2 m above the surface during the 23rd July. The aerosol measurements are 5 minute averages, made with a TSI3330 Optical Particle Sizer which counts and sizes particles from 0.3 to 10 μm diameter. Further information on the TSI3330 is given in Appendix D.

Fig. 5(a) demonstrates that around 1200 UT, the aerosol concentration starts to increase, reaching a max at 1330 UT. This is presumably due to the increase in daytime convection (supported by the relatively high vertical velocities in Fig. 4 at this time), which will easily loft particles upward. The extremely dry surface environment, characteristic of conditions which persist throughout the Mediterranean region in the summer months, means that particles are only very loosely bound to the surface. If charged, it follows that these lofted particles will contribute to the increased charge levels observed during the 1420 UT ascent. Fig. 5(a) also shows that most of the contribution to the total aerosol concentration is from small particles (< 1 μm), which are the most easy to be lofted. There will also be a further contribution
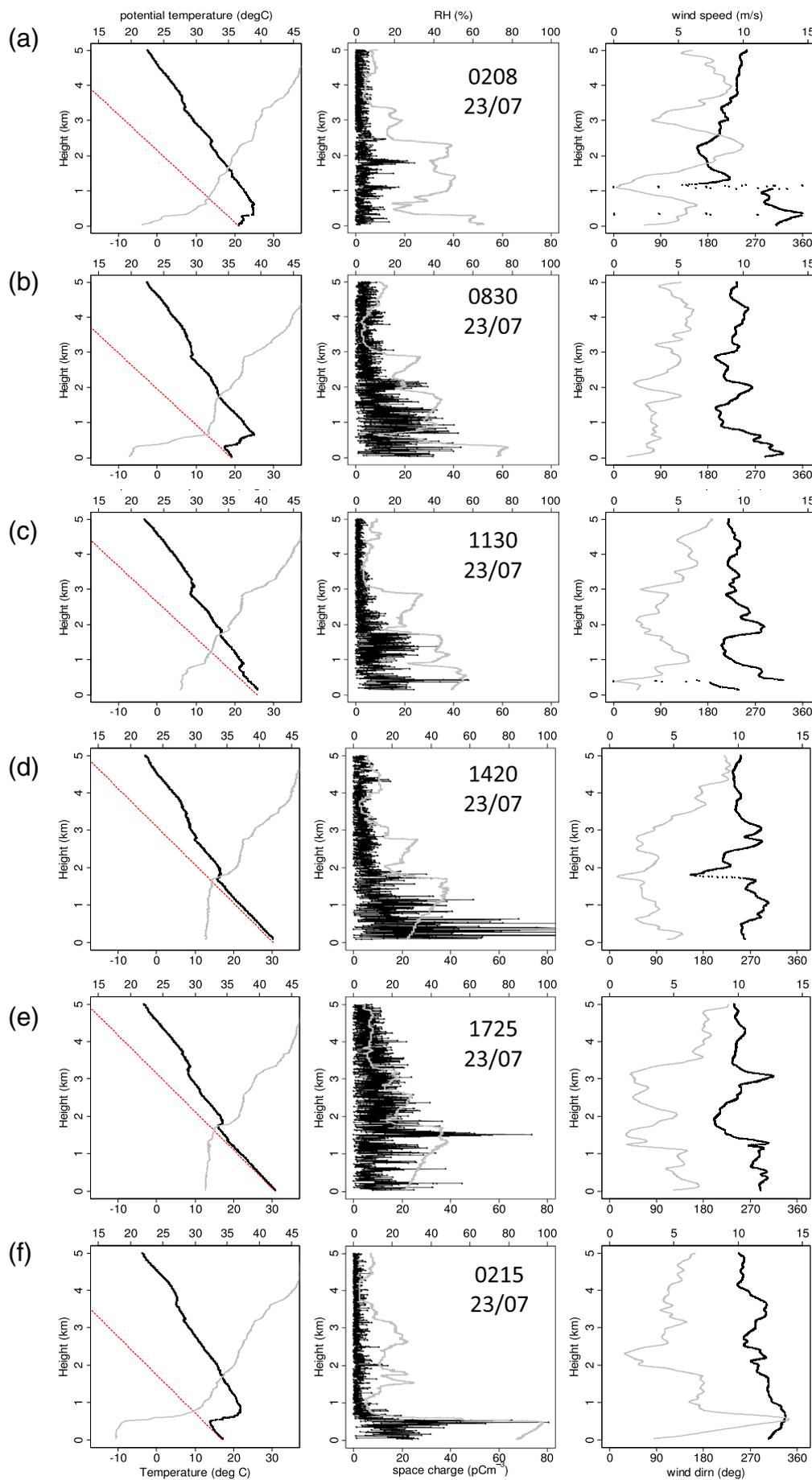
Fig. 2. Vertical profiles from specially instrumented radiosondes from (a) 0200 UT on 23rd to (f) 0200 UT on 24th July 2014. Each flight shows three plots. Left plot - temperature (black), potential temperature (grey) and Dry Adiabatic Lapse Rate (DALR) (red dashed); central plot - RH (grey), magnitude of space charge (black), Right plot - horizontal wind speed (grey) and wind direction (black). (For interpretation of the references to colour in this figure legend, the reader is referred to the web version of this article.)
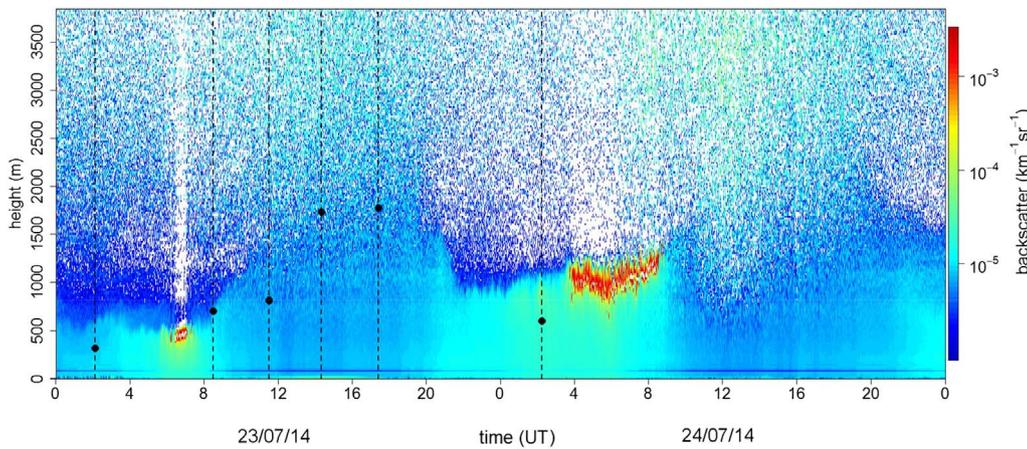
Fig. 3. Backscatter profile from the Vaisala CL31 ceilometer on 23rd and 24th July 2014 at Alqueva. Dashed vertical lines indicate the times of specially instrumented sonde ascents, and the black dots represent the height of the largest potential temperature inversion as determined from the sonde. The red and yellow points between 0500–0700 UT on 23rd and 0400–0900 UT on 24th denote periods when cloud was present. (For interpretation of the references to colour in this figure legend, the reader is referred to the web version of this article.)

from particles smaller than the 0.3 μm detection limit of the TSI3330 which were too small to be detected. Further evidence for the involvement of aerosol in the elevated charge levels is also given by the PG measurements shown in Fig. 5(a) (black line). During the period of enhanced aerosol concentration from 1200 UT to 1600 UT the PG is much greater, up to 350 V/m, and more variable than at other times. The reason for this may be twofold: 1) the aerosol concentration is sufficient to reduce the air conductivity, thereby increasing the PG in accordance with Ohm's law (for a constant vertical conduction current); 2) the aerosol particles are charged, and their separation into positive and negative charge regions causes a change in the net PG. A combination of both effects will occur, but the relatively small aerosol concentrations (which indicate that the lower tropospheric air in the Alqueva region is very clean) are very unlikely to lead to such large variability in the PG through the conductivity route alone. It is therefore suggested that space charge generation results mostly from movement of charge carried by ultrafine particles, as well as ionic space charge. The wind speed measurements shown in Fig. 5(b) show a

gradual increase in near surface wind speed from 1200 UT onwards, supporting the lofting possibility. Dust particles are likely to charge through a variety of mechanisms including triboelectric charging (e.g. Lacks and Levandovsky, 2007) and investigators have previously observed substantial surface electric fields within desert dust storms (e.g. Esposito et al., 2016; Yair et al., 2016; Harrison et al., 2016; Silva et al., 2016). Although the particle concentration and wind speeds here are nowhere near as large as the values observed in storms, Fig. 7 (which shows modelled vertical velocities for 22nd July), does show a marked increase in vertical velocity (up to 1 ms^{-1} at the surface) around the period of the maxima in aerosol concentration from 1400 UT to 1800 UT which could certainly loft surface aerosol through convective updrafts (e.g. Adler and Kalthoff, 2014). The predicted vertical velocities of up to 1 m/s would enable particles at the surface to be transported upwards to the maximum observed altitude of charging at 500 m in around 8 min (assuming that the particles travel at the same speed as the updrafts). There may also be an additional contribution to aerosol above the surface from long range horizontal advection from the North
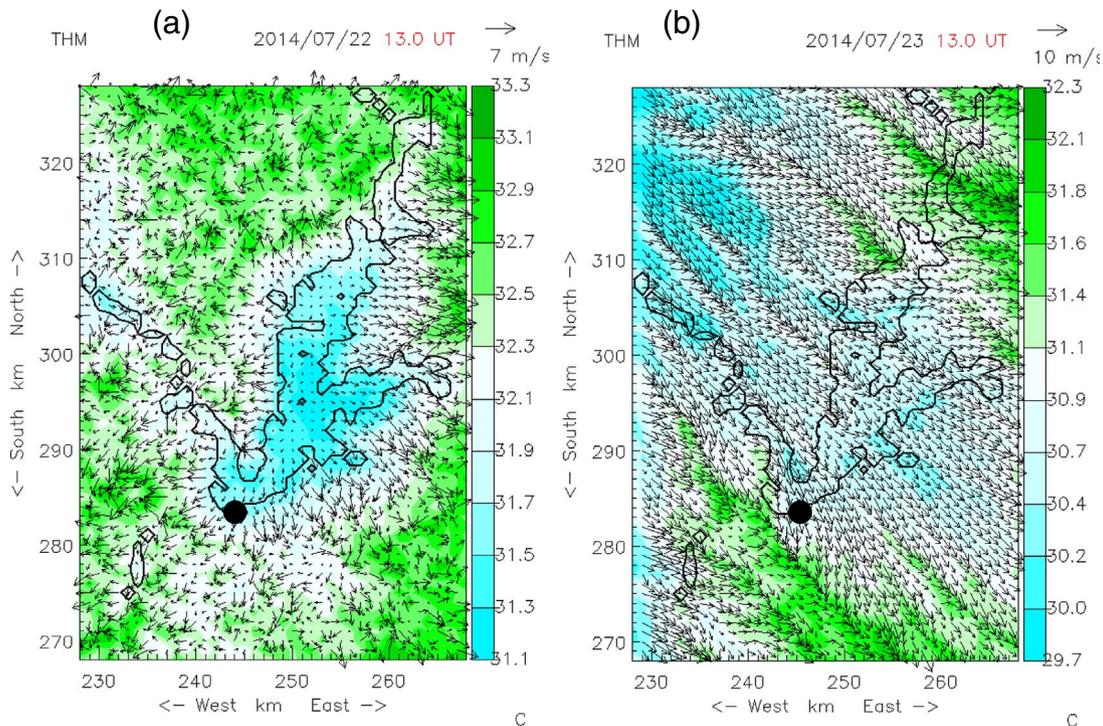
Fig. 4. Modelled horizontal wind (arrows) over potential temperature (coloured contours) in a model surface ~200 m above surface around Alqueva reservoir using the Meso-NH model with a resolution of 1 km at 1300 UT on (a) 22nd and (b) 23rd July. (For interpretation of the references to colour in this figure legend, the reader is referred to the web version of this article.)
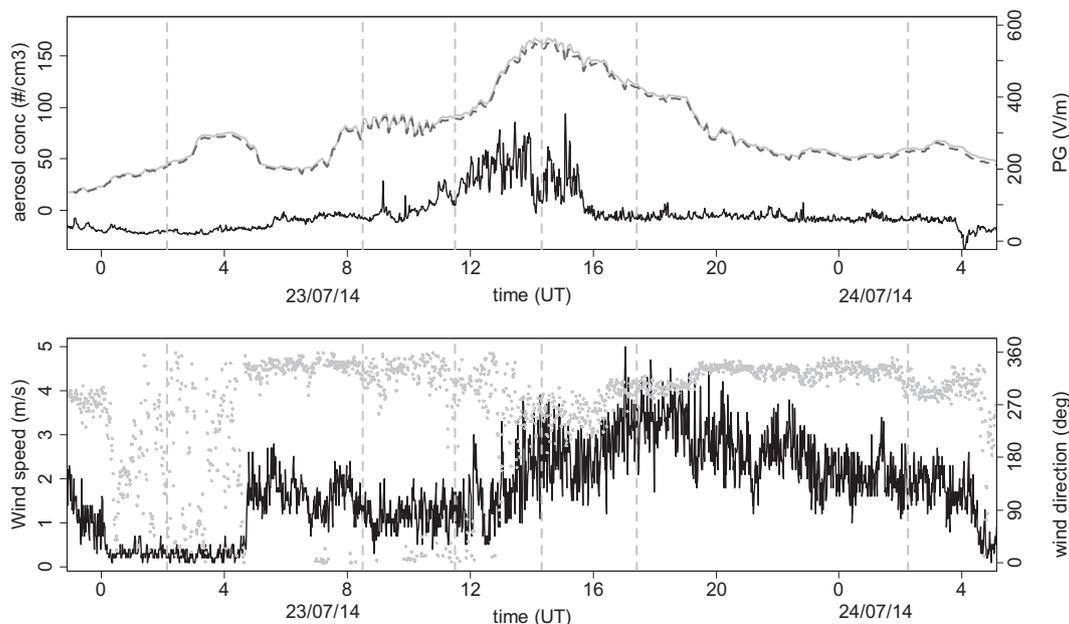
Fig. 5. (a) Aerosol number concentration (solid light grey = total concentration for all particles from 0.3–10 μm, dashed dark grey = concentration of particles < 1 μm), measured by a TSI3330 OPC. The black line shows measurements of Potential Gradient (PG) measured by a JCI 131F electric field mill. (b) 2 m wind speed (black solid line) and wind direction (grey points), all measured at Alqueva, Portugal on 23rd and 24th July 2014. Dashed grey lines denote the times of balloon ascents. Aerosol measurements are 5 minute averages, PG 1 minute averages and wind data 1 minute average.

Westerly flow which will have passed close to polluted cities such as Lisbon.

The movement of charged aerosol has been observed to cause rapid variations in PG (e.g. Matthews et al., 2012; Piper and Bennett, 2012; Conceição et al., 2017), very similar to those observed during 23rd July at Alqueva, therefore this is suggested as the cause of the unusually high variability in the PG during this period. The relationship between the surface PG and vertical charge profile will be discussed further in Section 3.2.

Returning to Fig. 2, Fig. 2(e) shows the vertical profile from the late afternoon ascent at 1725 UT. The temperature profile is almost identical to the 1420 UT ascent, suggesting a well-mixed atmosphere as before. The intense region of charge in the lower levels at 1420 UT is no longer present, instead a distinct charge layer exists between 1.5 and 2 km near the top of the boundary layer. This is suggested to result from the upward mixing of the surface lofted charge due to convection. By the time of the final vertical ascent at 0215 UT on 24th July (Fig. 2(f)), substantial surface cooling has led to an increase in the near surface RH up to 80% (this later led to the formation of a cloud layer, but not until 0330 UT). A well-defined charge layer is present in the region of high RH, related to hygroscopic growth of ions and aerosol, as in the previous night's ascent. The substantial temperature inversion at the top of this layer will lead to a sharp gradient between the moist air below and relatively dry air above, leading to charging of the particles as a result of flow of the vertical conduction current. This is likely to be the main source of charge for the flight shown in Fig. 2(f), which will be discussed further in Section 3.3.

To summarise the diurnal variation in the vertical charge profiles over Alqueva, it is observed that, as expected, the magnitude of the charge during night time profiles is much smaller (up to 20 pC m^{-3}) than during daylight hours (up to 92 pC m^{-3}). Considerable complexity in the charge profiles is observed once daytime convection begins, with lofting of ultrafine surface aerosol suggested to be the main contribution to the charge profile in the lowest 1 km. Early morning formation of thin cloud layers is also a source of charge separation through conduction current charging of droplets and aerosols at the upper and lower horizontal boundaries. Remnant effects of such charging can be seen several hours before and after the cloud becomes visible from

ceilometer measurements, i.e. charge separation occurs during the cloud formation processes and remains after the droplets have evaporated.

3.2. Surface electrical measurements

This section examines more closely the effect of charges aloft on the surface PG by considering the integrated columnar charge. We define the columnar space charge, ρ_c, as the sum of all space charge layers above the measurement point. In practise we represent this as:

$$\rho_c = \sum_{m=0}^{m_\infty} \rho_m,$$

(2)

where ρ_m is the space charge associated with the mth layer measured above the surface, and m_∞ is the uppermost layer considered. Fig. 6 shows a PG time series (black line) for the entire duration of the two day IOP covering all eight balloon flights (from 22nd July to 24th). Also plotted (red dots) are the integrated space charge totals from the surface up to 5 km, for each of the 8 charge sensor flights, using Eq. (2). Further discussion of the choice of 5 km as the height of the upper boundary is given in Appendix B. Fig. 6 shows that although there is some variability, it is generally the case that the integrated space charge profiles follow the same trend as the near surface PG, particularly around the time of the increased aerosol concentration around 1200 UT on 23rd as discussed in Section 3.1. This demonstrates the importance of the link between the surface electrical environment and aloft. Also shown in Fig. 6 (grey dot-dashed line) is the average diurnal variation in PG at Alqueva on fair weather days for the entire duration of the Alex campaign (from 26th May to 27th September). The difference between the PG on 23rd (0900 UT to 1500 UT) and the average PG curve demonstrates the likelihood of enhanced space charge production on this day which is characterised by an increase in the magnitude (279 V/m compared to 93 V/m) and variability. This is in contrast to the similarity observed between the average curve and PG measured on 22nd, indicating a typical fair weather day. It is suggested that the differences result from a change in wind conditions at the site and thus aerosol concentration between the two days. The 22nd is dominated by a local lake breeze (as demonstrated in Fig. 4(a)), with wind flowing outwards
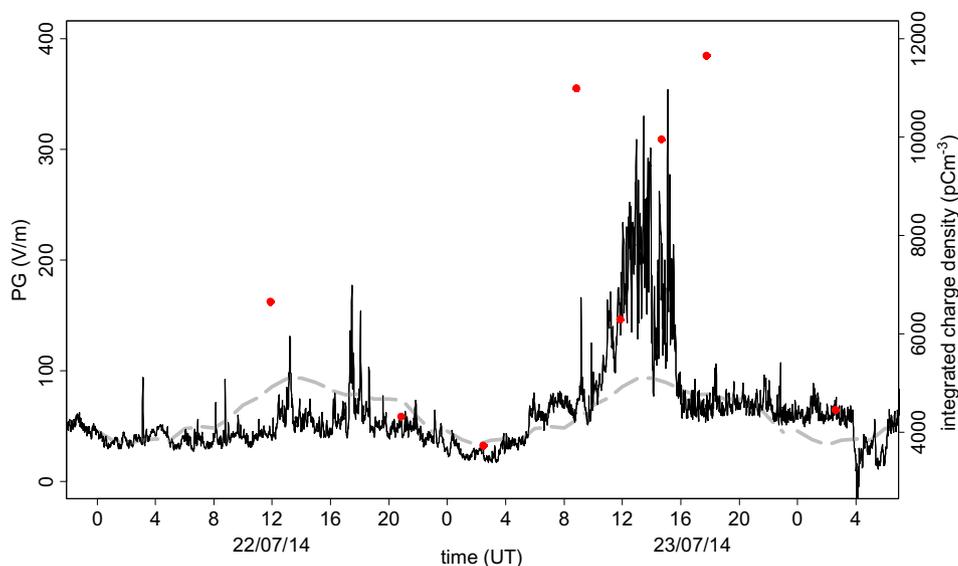
Fig. 6. Time series during the two days of the Alqueva IOP from 22nd to 24th July 2014. The black line denotes the PG, whilst the red dots show the calculated integrated space charge up to 5 km for each charge sensor balloon flight during the period (using Eq. (2)). The grey dash-dotted line show the averaged diurnal variation in PG for fair weather days at the Alqueva site during the entire ALEX campaign. (For interpretation of the references to colour in this figure legend, the reader is referred to the web version of this article.)
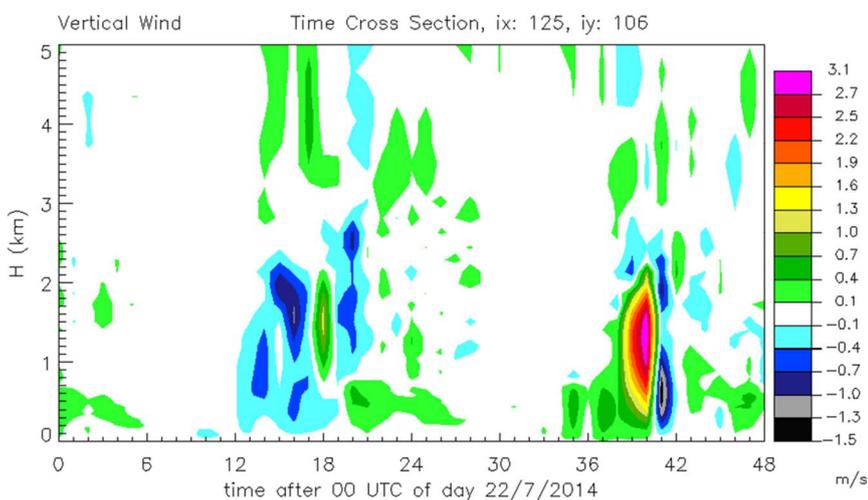
Fig. 7. Hovmöller plot of the vertical profile of Meso-NH modelled vertical velocity over the grid point nearest to the Parque Solar site at Alqueva, during 22nd and 23rd July.

from the lake towards the shore. This would contain relatively few aerosol particles (as supported by Fig. 5(a)), and the predominantly descending air over the lake body will inhibit vertical lofting of local aerosol at the PG measurement site. This is demonstrated in Fig. 7 which shows modelled time evolution of vertical velocity at Alqueva during 22nd and 23rd July, where it is evident that the vertical velocities on 22nd afternoon (12–18 UTC) are slightly negative (descending) in the boundary layer over the lake due to the development of the lake-breeze system. The fair weather conditions, low wind speeds and low aerosol content would lead to a predominately Carnegie like variation in PG as observed. This is contrasted with the predominantly north westerly wind flow on 23rd, which inhibits the formation of the lake breeze and therefore does not suppress the afternoon mesoscale convection. In addition, the circulation on 23rd is also likely to advect aerosol from more populated and industrialized coastal cities such as Lisbon The higher aerosol concentration on 23rd would increase the PG by both (a) reducing the conductivity and (b) causing an increased contribution to space charge by movement of charged aerosol. The presence of (b) is supported by the large variability in PG during peak convective hours.

Another factor that can cause variation in the PG and charge profiles is a change in the local ionisation. The vertical ionisation profile depends on both GCR ionisation generated from above and radioactivity from Earths' surface, mostly in the form of gamma radiation. Surface

measurements of gamma radiation were made during the ALEX campaign at Alqueva and reported by Lopes et al. (2015). These measurements corroborated the initial assumption that the Alqueva region emits very little gamma radiation, with no diurnal cycle evident in the measurements. The low geomagnetic latitude of Alqueva suggests that the variability in the near surface ionisation profile from GCRs will also be small (e.g. Bazilevskaya et al., 2008), hence it is extremely unlikely that variations in ionisation rate contributed to the observed changes in PG and space charge during 23rd July at Alqueva.

3.3. Charge modelling

Particulate aerosol is known to have a profound effect on the electrical environment, both at the surface and aloft (e.g. Sagalyn and Faucher, 1954; Gringel and Muhleisen, 1978). It is therefore desirable to know the vertical aerosol profile in order to better understand the vertical charge profile. Although measurements of aerosol were made at the surface during the Alqueva IOP, none were made in-situ aloft. Backscatter profile measurements were, however, made from a nearby Vaisala CL31 ceilometer. Although ceilometers are normally used for cloud detection, they can also be used for aerosol profiling (Münkel et al., 2004; Tsaknakis et al., 2011), and their ability to measure close to the surface is a distinct advantage over lidars, despite the lower pulse energy of ceilometers. Previous investigators (e.g. Münkel et al., 2004)
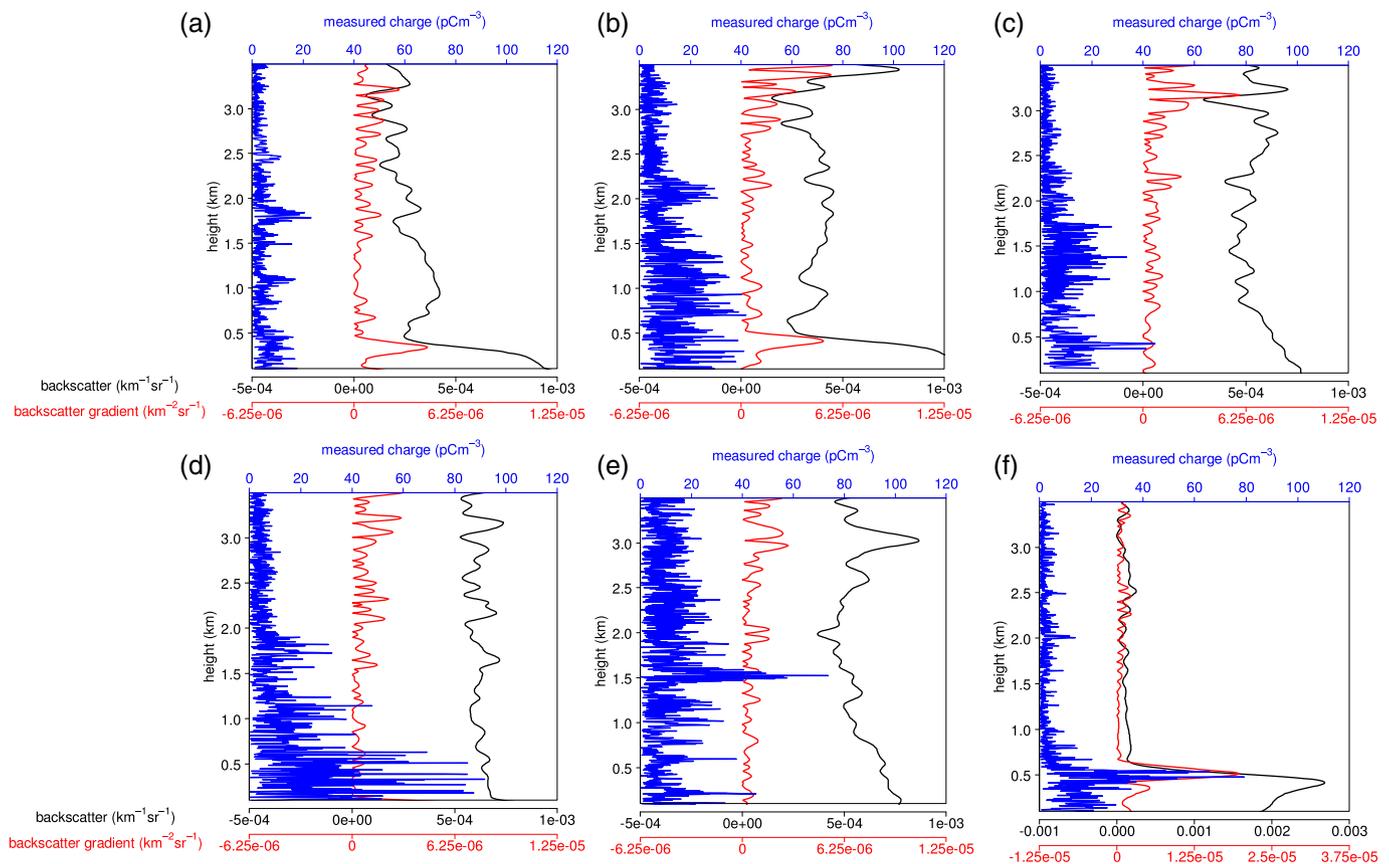
Fig. 8. Vertical profiles of the magnitude of space charge (blue) measured by the balloon charge sensor, processed backscatter from the surface ceilometer (black) (see Appendix C for details) and the magnitude of the vertical gradient in backscatter (red), which is indicative of the location of theoretically expected charge layers. Individual plots denote sonde flight times on 23rd and 24th July as follows: (a) 0208 UT, (b) 0830 UT, (c) 1130 UT, (d) 1420 UT, (e) 1725 UT, (f) 0215 UT. (For interpretation of the references to colour in this figure legend, the reader is referred to the web version of this article.)

have attempted to correlate ceilometer backscatter with surface aerosol measurements, however, artefacts in the backscatter profile have been demonstrated to occur in the ceilometer range gates providing information close to the surface, which reduces the usefulness of the comparison with ground based aerosol measurements. We therefore use the shape of the ceilometer backscatter profile as a qualitative indicator of the aerosol location, rather than attempt to infer anything quantitative about the aerosol concentration. Further discussion on the ceilometer instrument and the method used to process the ceilometer data is provided in Appendix C.

Fig. 8 shows the processed backscatter profiles (black line and detrended according to the methodology outlined in Appendix C) plotted alongside the measured charge profiles for each of the balloon flights in Fig. 2. In general, there is not much similarity observed between the charge and ceilometer backscatter profiles. Common features of the backscatter profiles are an increased layer of backscatter within approximately the lowest 800 m, particularly during night time and early morning hours (e.g. Fig. 8(a), (b) and (f)). This is related to the hygroscopic growth of aerosol (e.g. Silva et al., 2015), which results from the strong cooling overnight, eventually leading to cloud formation. As mentioned in Section 3.1, charge accumulation is expected to occur at the upper and lower horizontal boundaries of cloud and aerosol layers due to vertical flow of the GEC conduction current, J_c. The space charge is proportional to the vertical gradient in conductivity between the clear and aerosol laden air, which theoretically, produces positive charge at the top of the layer and negative charge at the base (see e.g. Nicoll and Harrison, 2016). If one assumes a mostly static situation, with no vertical mixing (which is only likely to occur here overnight when vertical ascent rates are low (e.g. Fig. 4)), a theoretical estimate of the charge generated by this phenomenon can be made by calculating

the vertical gradient in conductivity (see e.g. Harrison and Carslaw, 2003, Nicoll and Harrison, 2016 for details). However, the extent to which the charge values are realistic is questionable due to the absence of a quantitative aerosol profile and the number of assumptions required to do this. Instead the approach taken here is simply to calculate the vertical gradient in backscatter, which avoids the need for the many assumptions but will indicate the location of any charge layers thought to be generated by gradients in conductivity. Accordingly, the red line in each of the plots in Fig. 8 shows the vertical gradient in backscatter, which is indicative of the theoretical profile of charge. The vertical gradient is found by applying a smoothing spline (smoothing parameter = 0.3) to the backscatter and differentiating. As was the case for the backscatter profile, for most of the flights there is little similarity between the backscatter gradient and the observed charge. The likely reason for this is low sensitivity and 910 nm IR operating wavelength of the ceilometer which will lead to an inability to detect small particles (< 1 μm) and low particle concentrations. This is particularly important if the space charge is mostly ultrafine (i.e. diameters < 0.1 μm) rather than particulate. Since the surface aerosol measurements at Alqueva showed a predominantly clean atmosphere, it is expected that the sensitivity of the ceilometer will not detect such small particle concentrations. It should also be noted that the application of the vertical gradient in conductivity approach to a non-static situation in which turbulent motion is present over-simplifies the charge mixing processes taking place. Although charge will be separated at the upper and lower horizontal edges of aerosol layers due to this process, in a turbulent situation (such as during Fig. 8(c), (d) and (e)), the charge will be mixed vertically, leading to less well defined charge layers, which is more similar to that observed in the profiles in Fig. 8.

The one flight in which the shape of the backscatter profile is very

similar to the measured charge is Fig. 8(f). Fig. 9 shows a close up of the lowest 1.5 km of this flight, which demonstrates that a substantial gradient in backscatter occurs at 500 m altitude, which is coincident with the measured charge layer. The increased backscatter during this period is likely related to the later formation of a cloud layer which resulted from night time cooling under clear skies. The ceilometer algorithm did not classify this as a cloud until 0335 UT, more than an hour after the balloon measurements, therefore the profile shown in Fig. 9 was obtained before the cloud formed. The charge measurements and vertical gradient in backscatter in Fig. 9 are of both polarities (not simply magnitude as for the other plots), which demonstrates very close agreement between the location of the large backscatter gradients and the observed charge. Fig. 9 also shows the negative charge observed in the base of the layer and positive charge at the top, as expected by the theory of conduction current flow through aerosol and cloud layers (e.g. Zhou and Tinsley, 2007). Analysis of the data in Fig. 8 therefore suggests that this charging theory is valid for stratiform layers of aerosol and cloud, when the particle/droplet concentration is substantial and little vertical mixing is present, but not when substantial convective motion exists.

4. Discussion

From the results presented here it is apparent that the vertical profile of charge within the PBL can be complex, even in fair weather conditions. The analysis presented in Section 3 suggests a considerable influence for local charged aerosol on both the near surface PG measurements and vertical charge profile. Although the surface particle measurements and ceilometer backscatter profiles suggest relatively small aerosol particle number concentrations it is likely that larger concentrations of ultrafine ($< 0.1 \mu m$) particles and ionic space charge exist which will influence the charge distribution but will not be detected by either the ceilometer or surface particle counter. The ceilometer wavelength of 910 nm means that only particles greater than about 1 μm diameter will be detected, and only if the signal to noise is sufficiently large to permit a reliable signal to be measured. It is well documented that the day time signal-to-noise ratio in ceilometers in regions of low aerosol content is often poor (e.g. Heese et al., 2010),

which is consistent with the findings reported here in that there is little structure in the ceilometer backscatter profile except during night time and periods of high humidity. Although there is no observational evidence for these ultrafine particles, we can infer their existence from the measurements of elevated space charge values, i.e. in order for charge to be maintained beyond the timescale for recombination effects, the charge must be carried on larger particles. This is most likely to result from attachment to ultrafine particles.

The measurements reported here also demonstrate the importance of daytime convection for the vertical space charge profile within the PBL. At Alqueva this is particularly evident in terms of the ability of turbulent updrafts to transport small aerosol particles from the surface, which occurs easily and mixed primarily due to the extreme dryness of soil. This leads to relatively large values of space charge (up to 100 pC m^{-3}), in comparison to those reported by other observers in less dry environments (e.g. ~ 1 pC m^{-3} measured by Moore et al., 1962). In the absence of cloud layers, the largest values of space charge are observed during mid-afternoon when the vertical velocity is maximum and turbulent motion largest. Section 3.2 demonstrates clearly the difference in the electrical environment on days when convection is inhibited (such as on 22nd July when the lake breeze was present), and when it is not. This leaves little doubt that the main influence on the detailed structure of the vertical space charge profile at Alqueva is turbulent transport.

The relatively large values of space charge density reported here compared to other papers (e.g. of a few pC m^{-3} in Moore et al., 1962, Markson, 1975) may also result from differences in the measurement techniques as well as time resolution of the measurements. Markson (1975) and Markson et al. (1981) report measurements approximately every 200 m in the vertical, with no detail of any averaging or smoothing that has been applied. It may well be the case that this is an average value over 200 m rather than an instantaneous value. It is therefore likely that, in comparison to the approximately 5 m vertical resolution measurements reported here, the longer averaging periods reported in the literature resulted in smaller reported values of space charge. This therefore demonstrates the importance of high resolution measurements in understanding the detail of charge transfer within the boundary layer.

5. Conclusions

These results present rare high resolution vertical profiles of space charge within the planetary boundary layer, which are the first to be made over an inland Portuguese reservoir. The direct space charge determination reveals the complex structure of the vertical charge profiles, beyond that available indirectly from aerosol particle retrievals or thermodynamic inferences alone, which indicates the importance of charged ultrafine aerosol in the electrical environment of the boundary layer. Intensive balloon measurements over a 24 hour period of fair weather demonstrate variation of the charge profile within the planetary boundary layer and its dependence on convective mixing. The magnitude of observed charge is typically small during night time periods (up to 20 pC m^{-3}), with little vertical structure. Daytime convection leads to substantial vertical mixing, including lofting of aerosol particles upwards from the dry surface, which leads to substantial charge accumulations up to 92 pC m^{-3} within the lowest km. The diurnal variation in the integrated column of charge above the measurement site closely matches the diurnal variation in near surface charge as measured by an electric field mill at the same site. Vertical profiles of backscatter from an adjacent CL31 ceilometer were used to provide a proxy for the vertical aerosol profile, to which the measured charge profiles were compared. Little similarity between the two was observed, except during stable night time periods when reasonable aerosol layers accumulated. Most of the discrepancy is attributed to the likely existence of ultrafine aerosol (< 1 μm) which are too small to be detected by the ceilometer, but will contribute to the overall charge profile. Using such direct space charge measurements, the charge transfer processes can be identified and characterised, the variability in which is clearly apparent even in fair weather conditions. The simplicity with which these measurements can be obtained using conventional meteorological radiosondes therefore offers a new tool for improving boundary layer representations within radiative transfer models.

Appendix A. Meso-NH model

A map of southern Portugal with the orography, the Alqueva reservoir and the location of the Parque Solar measurement site during the ALEX 2014 campaign is provided in Fig. A1. Further maps of the Alqueva and the ALEX measurement stations may be found in Potes et al., 2017. In order to characterise the wind direction and evolution of the vertical profile of the vertical velocity at Alqueva, the results of a high resolution numerical simulation with Meso-NH model (Lafore et al., 1998) were used. The Meso-NH is a non-hydrostatic anelastic numerical model which includes several parametrization schemes to represent surface-atmosphere interactions, radiation, clouds and precipitation, convection, atmospheric electricity, chemical reactions and aerosols. The model was run over two two-way nested domains, the farther (not shown) covering all the Iberian Peninsula and adjacent ocean at 4 km horizontal resolution (270 × 240 grid points). The finer domain is centred over the Alqueva reservoir and covers the Portuguese Alentejo region at a 1 km horizontal resolution (240 × 240 grid points) and is shown in Fig. A1 alongside with the location of Alqueva artificial lake. The simulation was started on July 21st at 1800 UT and the initial and boundary conditions were provided by the 6 hourly ECMWF analysis. For the surface, the SURFEX platform of schemes (Masson et al., 2013) were used, the water temperature at Alqueva reservoir was initialized by the temperatures obtained from MODIS satellite data, and an interactive lake model, the Flake, was activated as described in Salgado and Le Moigne (2010). To map the model surface, the ECOCLIMAP v2.0 (Masson et al., 2003) updated by Policarpo et al. (2017) was used. In the inner domain the convection is assumed to be explicitly resolved (no shallow or deep convection schemes were activated) and the turbulence was parametrized using the 1D scheme of Cuxart et al. (2000). The meso-NH results shown in this work came from the inner model (1 km resolution).

Appendix B. Integrated space charge profiles

This section provides further discussion of the integrated columnar charge discussed in Section 3.2. To calculate the integrated columnar charge it was decided to apply Eq. (2) up to a maximum height of 5 km as the majority of the space charge (90%) lies beneath this height. To demonstrate that the choice of this value is not important for the qualitative interpretation given, Fig. B1 shows the integrated space charge from the surface up to 2, 3, 4 and 5 km. It can be seen that the shape of the integrated charge time series is invariant of the value of maximum height chosen.

Appendix C. Ceilometer features and processing of the backscatter profiles

After a brief description of the ceilometer system, this section provides detail on the processing applied to the ceilometer backscatter data for Figs. 8 and 9, as a well as a discussion of the value of the shape of the profile.

The CL31 Vaisala ceilometer uses a single lens design, meaning that the centre of the lens is used for collimating the outgoing laser beam, whereas the outer part of the lens is used for focusing the backscattered light onto the receiver. The separation between transmitting and receiving areas is

provided by an inclined mirror with a hole in the centre. In this way very good performance is achieved, even at low altitudes. The ceilometer has a measurement range from 0 to 7.5 km, maximum reporting resolution of 5 m and programmable measurement cycle (from 2 to 120 s). It uses an eye-safe laser InGaAs diode emitting at 910 nm.

The backscatter signal obtained in clear sky conditions is mainly due to aerosols. Assuming that these particles are mostly concentrated in the mixing layer and that their concentrations above are much lower, it is then reasonable to expect an accentuated decrease of the backscatter signal at the top of the mixing layer. This is true for most situations, except in the case of intense aerosol events.

Although it is possible to use surface aerosol data to attempt to calibrate the ceilometer, for the Vaisala CL31 ceilometer at the Alqueva site, a distinct local minimum in the backscatter was evident at 40 m (4th range gate) in all backscatter profiles. This has also been detected by other investigators (e.g. Sokół et al., 2014) and is an artefact, potentially caused by incomplete optical overlap, or software corrections introduced by the ceilometer manufacturer (see e.g. Kotthaus et al., 2016). Although reasonable agreement between the surface OPC aerosol measurements and the backscatter from the lowest 2 ceilometer range gates (10 m and 20 m) was found at Alqueva, the artefact at 40 m makes it questionable to attempt any calibration between surface data and backscatter values beneath 70 m, which is typically the lowest altitude thought to be free from overlap issues.

In order to analyse the backscatter profile above 40 m, one must also take account of the errors inherent in the backscatter measurement and the processing already undertaken by the ceilometer manufacturer. The grey points in Fig. C1(b) show the vertical profile of backscatter during daylight conditions (0830 UT) on 23rd July (flight 4) at Alqueva, which appear reasonable in the lowest 1 km of the profile, but show an unphysical increase with height above this, as well as an increase in variability. This is apparent in all of the backscatter profiles coinciding with the radiosonde flights and is thought to be erroneous, due to noise from varying solar radiation as well as electronic and optical noise in the ceilometer. To extract a quantitative backscatter profile it is necessary to remove some of the noise by correcting the raw backscatter profile. This is achieved by producing an average background night time climatology profile (shown in black in Fig. C1(a)) from Alqueva, which should be devoid of any noise from solar radiation. This is calculated by finding the mean backscatter profile for all times from 0000 UT to 0300 UT from 22nd to 24th July 2016. Since the backscatter is typically highly variable within the PBL, this profile is therefore only calculated for altitudes above 800 m. The night time climatology profile is then scaled according to the maximum backscatter measured during any specific profile, and subtracted from the raw backscatter to produce a noise corrected version. A moving average (over 5 points) is then applied to the de-trended backscatter data to the processed backscatter, shown as the black line shown in Fig. C1(b). This process has been applied to the instantaneous backscatter profiles coincident with the six instrumented balloon flights shown in Fig. 2. It is also prudent to note the distinct decrease in the backscatter at 2.4 km observed for all Alqueva profiles (as seen in Fig. C1(a)), which is another artefact introduced in the processing by the manufacturer. This has been previously reported by Kotthaus et al. (2016) as likely due to a difference in averaging of data below and above this height. It is clear that removal of such artefacts (as is achieved by subtracting the scaled night time climatology profile) is vital to obtain reliable, quantitative backscatter measurements.

Appendix D. OPS 3330 features and particle concentration calculation

The Optical Particle Sizer (OPS) 3330, manufactured by TSI, is based on the principle of optical scattering from single particles. A laser beam shaped to a thin sheath focused below the inlet nozzle illuminates the particles entering the inlet nozzle. As particles pass through this light sheath, they scatter light in the form of pulses that are counted and sized simultaneously. Sheath flow keeps the particles well focused across the laser light and also prevents the optics from getting contaminated. Beam shaping optics focus the laser light and convert that to a fine sheath with maximum intensity across the particle beam. The viewing volume is created by the intersection of the laser sheath and the particle flow. Sophisticated electronics are used to perform the signal processing. Particle pulses are counted individually and binned in to the 16 channels of the detector, based on their pulse heights. The maximum particle size that can be counted is 10 μm, particles larger than this will be counted but not sized.

The OPS measures particle concentration counting individual pulses from the photodetector. When, pulses start to overlap each other, meaning high particle concentrations, the number of pulses underestimates the number of particles entering the viewing volume. When a particle is detected entering the optical viewing volume, no other particles can be counted until that particle leaves the viewing volume. As the particle concentrations increase, the amount of time blocked by the presence of particles becomes significant. If the particle concentration is computed using elapsed time, the value will be under reported. The actual sample time needs to be corrected for this blocked or dead-time. To adjust for this effect, the OPS measures the dead-time resulting from the presence of particles in the viewing volume and subtracts it from the sample time. This sample lifetime value is used in place of the sample time for the concentration calculations as in the following formula.

$$C_i = \frac{N_i}{Q \times (t_s - DTC \times t_d)}, \tag{D1}$$

where,

C_i = concentration at size channel i
N_i = number count in #/cm^3 at size channel i
Q = sample flow rate, 16.67 cm^3 s^{-1}
t_s = sample time in seconds
t_d = dead time in seconds
DTC = dead time correction factor
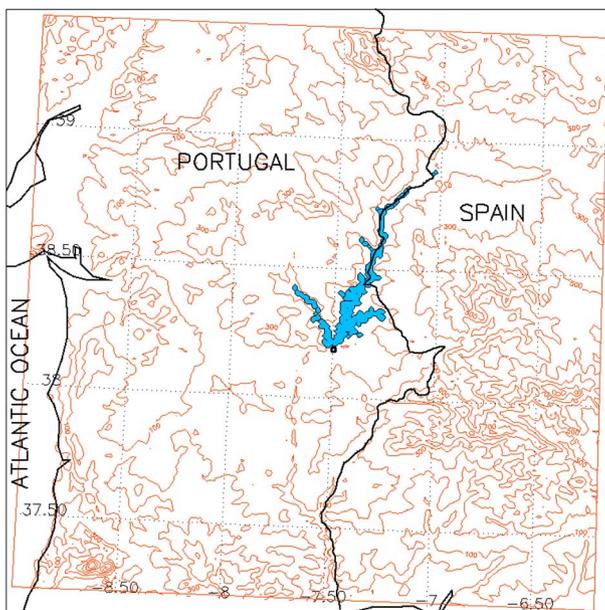
Fig. A1. Domain and orography at 1 km horizontal resolution used in the inner model of the Meso-NH simulation (contour intervals of 100 m). The Alqueva reservoir, as used in the simulations is shown in blue. The location of the Parque Solar (PS) site at which the PG and balloon measurements were made is represented by the black circle. (For interpretation of the references to colour in this figure legend, the reader is referred to the web version of this article.)
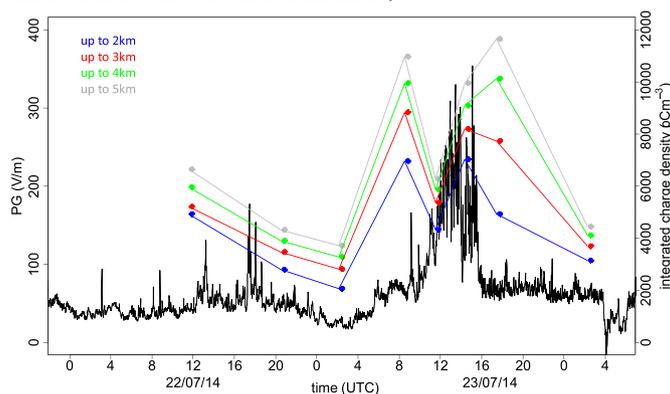
Fig. B1. Time series during the two days of the Alqueva IOP from 22nd to 24th July 2014. The black line denotes the PG, whilst the coloured red dots show the calculated integrated space charge up to 2 km (blue), 3 km (red), 4 km (green) and 5 km (grey) for each charge sensor balloon flight during the period (using Eq. (2)). (For interpretation of the references to colour in this figure legend, the reader is referred to the web version of this article.)
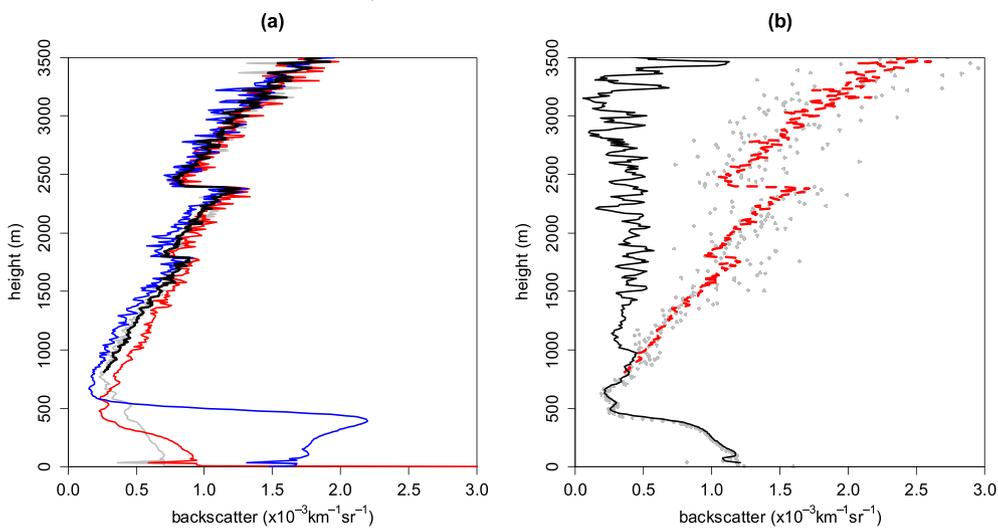
Fig. C1. (a) Average night time vertical profiles of backscatter from the CL31 ceilometer for nights of 22nd (grey), 23rd (red) and 24th (blue) July 2014 from 00 to 03 UT. The black line shows the mean of the three profiles, denoting the night time climatology. (b) Vertical profile of backscatter at 0830 UT on 23rd July (flight 4). The profile is the mean of a 30 minute window from the launch time. Grey points - raw backscatter, red – relative night time climatology profile, black – processed backscatter. (For interpretation of the references to colour in this figure legend, the reader is referred to the web version of this article.)

References

Adler, B., Kalthoff, N., 2014. Multiscale transport processes observed in the boundary layer over a mountainous island. Bound.-Layer Meteorol. 153, 515–537. http://dx.doi.org/10.1007/s10546-014-9957-8.

Anisimov, S.V., Bakastov, S.S., Mareev, E.A., 1994. Spatiotemporal structures of electric field and space charge in the surface atmospheric layer. J. Geophys. Res.-Atmos. 99 (D5), 10603–10610.

Anisimov, S.V., Mareev, E.A., Bakastov, S.S., 1999. On the generation and evolution of aeroelectric structures in the surface layer. J. Geophys. Res.-Atmos. 104 (D12), 14359–14367.

Anisimov, S.V., Mareev, E.A., Shikhova, N.M., Shatalina, M.V., Galichenko, S.V., Zilitinkevich, S.S., 2013. Aeroelectric structures and turbulence in the atmospheric boundary layer. Nonlinear Process. Geophys. 20 (5), 819–824.

Aplin, K.L., Harrison, R.G., 2013. Lord Kelvin's atmospheric electricity measurements. Hist. Geo Space Sci. 4, 83–95.

Bazilevskaya, G.A., Usoskin, I.G., Flückiger, E.O., Harrison, R.G., Desorgher, L., Bütikofer, R., Krainev, M.B., Makhmutov, V.S., Stozhkov, Y.I., Svirzhevskaya, A.K., Svirzhevsky, N.S., 2008. Cosmic ray induced ion production in the atmosphere. Space Sci. Rev. 137, 149–173.

Cavello, T., 1777. An account of some new electrical experiments. Philos. Trans. R. Soc. Lond. 67, 48–55.

Conceição, R., Silva, H.G., Bennett, A., Salgado, R., Bortoli, D., Costa, M.J., Collares Pereira, M., 2017. High frequency response of the atmospheric electric potential gradient under strong and dry boundary layer convection. Bound.-Layer Meteorol. http://dx.doi.org/10.1007/s10546-017-0298-2.

Crozier, W.D., 1963. Electrode effect during nighttime low-wind periods. J. Geophys. Res. 68 (11), 3451–3458.

Cuxart, J., Bougeault, P., Redelspergen, J., 2000. A turbulence scheme allowing for mesoscale and large-eddy simulations. Q. J. R. Meteorol. Soc. 126, 1–30.

Esposito, F., Molinaro, R., Popa, C.I., Molfese, C., Cozzolino, F., Marty, L., Taj-Eddine, K., Di Achille, G., Franzese, G., Silvestro, S., Ori, G.G., 2016. The role of the atmospheric electric field in the dust-lifting process. Geophys. Res. Lett. 43 (10), 5501–5508.

Garratt, J., 1994. The atmospheric boundary layer. Earth Sci. Rev. 37 (1–2), 89–134.

Gringel, W., Muhleisen, R., 1978. Saharan dust concentration in the troposphere over the North Atlantic derived from measurements of air conductivity. Beitr. Phys. Atmos. 51 (2), 121–128.

Harrison, R.G., 2013. The Carnegie curve. Surv. Geophys. 34 (2), 209–232.

Harrison, R.G., Aplin, K.L., 2003. Nineteenth century Parisian smoke variations inferred from Eiffel tower atmospheric electrical observations. Atmos. Environ. 37, 5319–5324.

Harrison, R.G., Carslaw, K.S., 2003. Ion–aerosol–cloud processes in the lower atmosphere. Rev. Geophys. 41 (3), 1012. http://dx.doi.org/10.1029/2002RG000114.

Harrison, R.G., Nicoll, K.A., Lomas, A.G., 2012. Programmable data acquisition system for research measurements from meteorological radiosondes. Rev. Sci. Instrum. 83, 036106. http://dx.doi.org/10.1063/1.3697717.

Harrison, R.G., Nicoll, K.A., Ambaum, M.H.P., 2015. On the microphysical effects of observed cloud edge charging. Q. J. R. Meteorol. Soc. 141, 2690–2699. http://dx.doi.org/10.1002/qj.2554.

Harrison, R.G., Barth, E., Esposito, F., Merrison, J., Montmessin, F., Aplin, K.L., Borlina, C., Berthelier, J.J., Déprez, G., Farrell, W.M., Houghton, I.M.P., Renno, N.O., Nicoll, K.A., Tripathi, S.N., Zimmerman, M., 2016. Applications of electrified dust and dust devil electrodynamics to Martian atmospheric electricity. Space Sci. Rev. http://dx.doi.org/10.1007/s11214-016-0241-8.

Heese, B., Flentje, H., Althausen, D., Ansmann, A., Frey, S., 2010. Ceilometer lidar comparison: backscatter coefficient retrieval and signal-to-noise ratio determination. Atmos. Meas. Tech. 3 (6), 1763–1770.

Hoppel, W.A., Frick, G.M., 1986. Ion—aerosol attachment coefficients and the steady-state charge distribution on aerosols in a bipolar ion environment. Aerosol Sci. Technol. 5 (1), 1–21. http://dx.doi.org/10.1080/02786828608959073.

Hoppel, W.A., Gathman, S.G., 1971. Determination of eddy diffusion coefficients from atmospheric electrical measurements. J. Geophys. Res. 76 (6), 1467–1477. http://dx.doi.org/10.1029/JC076i006p01467.

Hoppel, W.A., Gathman, S.G., 1972. Experimental determination of the eddy diffusion coefficient over the open ocean from atmospheric electric measurements. J. Phys. Oceanogr. 2 (3), 248–254.

Hoppel, W.A., Anderson, R.V., Willett, J.C., 1986. Atmospheric electricity in the planetary boundary layer. In: The Earth's Electrical Environment, pp. 149–165.

Israel, H., 1955. Synoptical researches on atmospheric electricity. In: Proc. Conference on Atmospheric Electricity, pp. 11–20.

Kaimal, J.C., Finnigan, J.J., 1994. Atmospheric Boundary Layer Flows: Their Structure and Measurement. Oxford University Press.

Kawano, M., 1957. The general expression of the diurnal variation of the atmospheric electric field considering the influence of the Eddy diffusion near the ground. J. Geomagn. Geoelectr. 9 (3), 123–132.

Kotthaus, S., O'Connor, E., Munkel, C., et al., 2016. Recommendations for processing atmospheric attenuated backscatter profiles from Vaisala CL31 ceilometers. Atmos. Meas. Tech. 9 (8), 3769.

Kulkarni, Madhuri N., 2010. On the modeling of electrical boundary layer (electrode layer) and derivation of atmospheric electrical profiles, eddy diffusion coefficient and scales of electrode layer. J. Earth Syst. Sci. 119 (1), 75–86.

Lacks, D.J., Levandovsky, A., 2007. Effect of particle size distribution on the polarity of triboelectric charging in granular insulator systems. J. Electrost. 65 (2), 107–112.

Lafore, J., Stein, J., Asencio, N., Bougeault, P., Ducrocq, V., Duron, J., Fischer, C., Hereil, P., Mascart, P., Pinty, J., Redelsperger, J., Richard, E., Arellano, J., 1998. The meso-nh atmospheric simulation system. Part 1: adiabatic formulation and control

simulation. Ann. Geophys. 16, 90–109.

Lopes, F., Silva, H.G., Bárias, S., Barbosa, S.M., 2015. Preliminary results on soil-emitted gamma radiation and its relation with the local atmospheric electric field at Amieira (Portugal). J. Phys. Conf. Ser. 646, 012015. http://dx.doi.org/10.1088/1742-6596/646/1/012015.

Lopes, F., Silva, H.G., Salgado, R., Potes, M., Nicoll, K., Harrison, G., 2016. Atmospheric electrical field measurements near a fresh water reservoir and the formation of the lake breeze. Tellus A 68, 31592. http://dx.doi.org/10.3402/tellusa.v68.31592.

Mach, D.M., Blakeslee, R.J., Bateman, M.G., 2011. Global electric circuit implications of combined aircraft storm electric current measurements and satellite-based diurnal lightning statistics. J. Geophys. Res.-Atmos. 116 (D5).

Markson, R., 1975. Atmospheric electrical detection of organized convection. Science 188 (4194), 1171–1177.

Markson, R., Sedlacek, J., Fairall, C.W., 1981. Turbulent transport of electric charge in the marine atmospheric boundary layer. J. Geophys. Res. 86 (C12), 12–115.

Marshall, T.C., Rust, W.D., Stolzenburg, M., Roeder, W.P., Krehbiel, P.R., 1999. A study of enhanced fair-weather electric fields occurring soon after sunrise. J. Geophys. Res. 104 (D20), 24–455.

Masson, V., Champeaux, J., Chauvin, C., Meriguet, C., Lacaze, R., 2003. A global database of land surface parameters at 1 km resolution for use in meteorological and climate models. J. Clim. 16, 1261–1282.

Masson, V., Moigne, P., Martin, E., Faroux, S., Alias, A., Alkama, R., Belamari, S., Barbu, A., Boone, A., Bouyssel, F., Brousseau, P., Brun, E., Calvet, J., Carrer, D., Decharme, B., Delire, C., Donier, S., Essaouini, K., Gibelin, A., Giordani, H., Habets, F., Jidane, M., Kerdraon, G., Kourzeneva, E., Lafaysse, M., Lafont, S., Brossier, C., Lemonsu, A., Mahfouf, J., Marguinaud, P., Mokhtari, M., Morin, S., Pigeon, G., Salgado, R., Seity, Y., Taillefer, F., Tanguy, G., Tulet, P., Vincendon, B., Vionnet, V., Voldoire, A., 2013. The surfexv7.2 land and ocean surface platform for coupled or offline simulation of earth surface variables and fluxes. Geosci. Model Dev. 6, 929–960.

Matthews, J.C., Buckley, A.J., Wright, M.D., Henshaw, D.L., 2012. Comparisons of ground level measurements of ion concentration and potential gradient upwind and downwind of HV power lines in corona. J. Electrost. 70 (4), 407–417.

Moore, C.B., Vonnegut, B., Semonin, R.G., Bullock, J.W., Bradley, W., 1962. Fair-weather atmospheric electric potential gradient and space charge over central Illinois, summer 1960. J. Geophys. Res. 67 (3), 1061–1071.

Münkel, C., Emeis, S., Müller, W.J., Schaefer, K.P., 2004. Aerosol concentration measurements with a lidar ceilometer: results of a one year measuring campaign. In: Remote Sensing. International Society for Optics and Photonics, pp. 486–496.

Nicoll, K.A., 2013. A self-calibrating electrometer for atmospheric charge measurements from a balloon platform. Rev. Sci. Instrum. 84, 096107.

Nicoll, K.A., Harrison, R.G., 2010. Experimental determination of layer cloud edge charging from cosmic ray ionisation. Geophys. Res. Lett. 37 (13).

Nicoll, K.A., Harrison, R.G., 2016. Stratiform cloud electrification: comparison of theory with multiple in-cloud measurements. Q. J. R. Meteorol. Soc. 142, 2679–2691. http://dx.doi.org/10.1002/qj.2858.

Piper, I.M., Bennett, A.J., 2012. Observations of the atmospheric electric field during two case studies of boundary layer processes. Environ. Res. Lett. 7 (1), 014017.

Policarpo, C., Salgado, R., Costa, M.J., 2017. Numerical simulations of fog events in southern portugal. Adv. Meteorol. 2017. http://dx.doi.org/10.1155/2017/1276784.

Potes, M., Salgado, R., Costa, M.J., Morais, M., Bortoli, D., Kostadinov, I., Mammarella, I., 2017. Lake–atmosphere interactions at Alqueva reservoir: a case study in the summer of 2014. Tellus A 1 (1272787), 69.

Reiter, R., Sládkovič, R., 1970. Control of vertical transport of aerosols between 700 and 3000 meters by lapse rate and fine structure of temperature. J. Geophys. Res. 75 (15), 3065–3075. http://dx.doi.org/10.1029/JC075i015p03065.

Rycroft, M.J., Harrison, R.G., Nicoll, K.A., Mareev, E.A., 2008. An overview of Earth's global electric circuit and atmospheric conductivity. Space Sci. Rev. 137 (1–4), 83–105.

Sagalyn, R.C., Faucher, G.A., 1954. Aircraft investigation of the large ion content and conductivity of the atmosphere and their relation to meteorological factors. J. Atmos. Terr. Phys. 5 (1), 253–272.

Sagalyn, R.C., Faucher, G.A., 1956. Space and time variations of charged nuclei and electrical conductivity of the atmosphere. Q. J. R. Meteorol. Soc. 82 (354), 428–445.

Salgado, R., Le Moigne, P., 2010. Coupling of the flake model to the surfex externalized surface model. Boreal Environ. Res. 15, 231–244.

Silva, H.G., Conceição, R., Wright, M.D., Matthews, J.C., Pereira, S.N., Shallcross, D.E., 2015. Aerosol hygroscopic growth and the dependence of atmospheric electric field measurements with relative humidity. J. Aerosol Sci. 85, 42.

Silva, H.G., Lopes, F., Pereira, S., Nicoll, K., Barbosa, S.M., Conceição, R., Neves, S., Harrison, R.G., Collares Pereira, M., 2016. Saharan dust electrification perceived by a triangle of atmospheric electricity stations in Southern Portugal. J. Electrost. 84, 106–120.

Sokół, P., Stachlewska, I.S., Ungureanu, I., Stefan, S., 2014. Evaluation of the boundary layer morning transition using the CL-31 ceilometer signals. Acta Geophys. 62 (2), 367–380.

Stull, R.B., 2012. An Introduction to Boundary Layer Meteorology. vol. 13 Springer Science & Business Media.

Tammet, H., 1995. Size and mobility of nanometer particles, clusters and ions. J. Aerosol Sci. 26 (3), 459–475.

Tsaknakis, G., Papayannis, A., Kokkalis, P., Amiridis, V., Kambezidis, H.D., Mamouri, R.E., Georgoussis, G., Avdikos, G., 2011. Inter-comparison of lidar and ceilometer retrievals for aerosol and Planetary Boundary Layer profiling over Athens, Greece. Atmos. Meas. Tech. 4 (6), 1261–1273.

Whipple, F.J.W., 1929. On the association of the diurnal variation of the electric potential gradient in fine weather with the distribution of thunderstorms over the globe. Q. J. R. Meteorol. Soc. 55, 351–362. http://dx.doi.org/10.1002/qj.49705523206.

Willett, J.C., 1979. Fair weather electric charge transfer by convection in an unstable planetary boundary layer. J. Geophys. Res. 84 (C2), 703–718. http://dx.doi.org/10.1029/JC084iC02p00703.

Willett, J.C., 1981. Toward an Understanding of the Turbulent Electrode Effect Over Land. No. NRL-8519. Naval Research Lab, Washington D.C.

Williams, E.R., 2009. The global electrical circuit: a review. Atmos. Res. 91 (2–4), 140–152. http://dx.doi.org/10.1016/j.atmosres.2008.05.018.

Wilson, C.T.R., 1921. Investigations on lightning discharges and on the electric field of thunderstorms. Philos. Trans. R. Soc. London, Ser. A 221, 73–115. http://dx.doi.org/10.1098/rsta.1921.0003.

Yair, Y., Katz, S., Yaniv, R., Ziv, B., Price, C., 2016. An electrified dust storm over the Negev desert, Israel. Atmos. Res. 181, 63–71.

Zhou, L., Tinsley, B.A., 2007. Production of space charge at the boundaries of layer clouds. J. Geophys. Res. 112, D11203. http://dx.doi.org/10.1029/2006JD007998.